Three-dimensional evaluation of gettering ability for oxygen atoms at small-angle tilt boundaries in Czochralski-grown silicon crystals

Yutaka Ohno,[1,a)] Kaihei Inoue,[1] Kozo Fujiwara,[1] Momoko Deura,[1] Kentaro Kutsukake,[1] Ichiro Yonenaga,[1] Yasuo Shimizu,[2] Koji Inoue,[2] Naoki Ebisawa,[2] and Yasuyoshi Nagai[2]
[1]*Institute for Materials Research (IMR), Tohoku University, Katahira 2-1-1, Aoba-ku, Sendai 980-8577, Japan*
[2]*The Oarai Center, IMR, Tohoku University, Oarai, Ibaraki 311-1313, Japan*

(Received 21 April 2015; accepted 14 May 2015; published online 23 June 2015)

Three-dimensional distribution of oxygen atoms at small-angle tilt boundaries (SATBs) in Czochralski-grown p-type silicon ingots was investigated by atom probe tomography combined with transmission electron microscopy. Oxygen gettering along edge dislocations composing SATBs, post crystal growth, was observed. The gettering ability of SATBs would depend both on the dislocation strain and on the dislocation density. Oxygen atoms would agglomerate in the atomic sites under the tensile hydrostatic stress larger than about 2.0 GPa induced by the dislocations. It was suggested that the density of the atomic sites, depending on the tilt angle of SATBs, determined the gettering ability of SATBs. © *2015 AIP Publishing LLC*. [http://dx.doi.org/10.1063/1.4921742]

More than 90% of photovoltaic cells are fabricated with crystalline silicon (Si). Most of the crystals are grown by the cast or Czochralski (CZ) method, by which a high concentration of oxygen atoms (up to 0.002 at. %) are introduced. Since the concentration is higher than the solubility limit at temperatures below about 1200 °C, oxygen atoms prefer to be precipitated, especially at lattice defects, such as grain boundaries, during crystal growth and device fabrication processes.[1–4] Unlike metallic impurities, oxygen atoms are difficult to be eliminated due to the precipitation effects.[3] Oxygen precipitates act as a recombination center, which deteriorates solar cell efficiencies.[5–7] Also, they would act as a gettering site for harmful metallic contaminants.[8,9] Moreover, they can introduce subsidiary defects such as dislocation arrays.[10] Since the density of oxygen precipitate nuclei seems to be the critical factor in regards to the degradation of solar cells,[8] oxygen atoms in isolation would be preferable for solar cell performance. Precise understanding of oxygen precipitation conditions is, therefore, one important issue for engineering the precipitates in controlled fashions,[11] in order to produce cost-effective functional cells.

Small-angle tilt boundaries (SATBs), composed of edge dislocations, whose density is determined by the tilt angle θ_{SATB} (less than about 10°),[12,13] are frequently introduced in cast Si,[3,14,15] as well as in directionally solidified Si[16,17] and Si ribbons,[4] during the crystal growth. They can also be introduced in device fabrication processes even in monocrystalline CZ-Si, from precipitates,[10] grain boundaries,[18] and stacking faults.[19] They can act as a sink for oxygen atoms,[20] and it is under the hypothesis that the boundaries with oxygen atoms would deteriorate solar cell efficiencies.[14] The gettering ability depends on θ_{SATB};[3] photoluminescence due to oxygen precipitates at SATBs is observed at $\theta_{SATB} \geq 1°$. In the present work, the origin of the θ_{SATB}-dependent oxygen gettering was examined.

Oxygen gettering processes are examined by analytical techniques based on transmission electron microscopy (TEM).[2] However, the initial stage of precipitation is not fully understood at atomistic levels, since oxygen precipitates smaller than a few nm in size are difficult to analyse by TEM (with an impurity detection limit of 0.05–0.1 at. % at most).[21] In the present work, three-dimensional (3D) distribution of oxygen atoms at SATBs was examined by atom probe tomography (APT), which has a low detection limit two orders lower than the limit by TEM (about 0.005 at. % in the present analyses), simultaneously with a spatial resolution comparable to the resolution of TEM (0.4 nm and 0.2 nm in lateral and depth resolutions at best).[22] Oxygen gettering along edge dislocations composing SATBs was observed, and the gettering ability was correlated with elastic strains due to the dislocations. This finding would help to control metallic contaminants by phosphorous diffusion gettering[23–25] and thermal[26] processes, disturbed by oxygen precipitates, as well as to engineer the distribution of oxygen precipitates at SATBs in controlled fashions.

One Si ingot (about 1 in. diameter) containing boron (0.01 at. %) and oxygen (0.002 at. %) atoms was grown with a bicrystal seed by the CZ method. The seed was prepared by combining two square-prisms of Si with nearly {100} surfaces ($2 \times 2 \times 50\,mm^3$), and it was pulled along [001] with a rate of 3 μm/s from a melt of granulated boron and Si. SATBs with the rotation axis of [001] were introduced accidentally in the ingot. Each SATB had a different tilt angle in the range from about 1° to 5°. A (001) surface of the ingot was etched with a reagent of $3HNO_3$:1HF at 20 °C, and a SATB was observed as a groove on the surface. Thin foils for TEM and needles for APT with the SATB were prepared by focused-ion-beam (FIB) milling under *in-situ* scanning electron microscopy.[27] The angle θ_{SATB} of the SATB was analysed by electron back scattered diffraction (EBSD) before FIB, and it was confirmed by TEM. 3D distribution of oxygen atoms at the SATB was examined with a local electrode atom probe (Ametek, LEAP4000X HR). The ratio of the doubly charge state to the singly one for Si was more than 150, with the same experimental condition as in the previous report.[27] 3D maps of oxygen atoms were reconstructed

[a)]Electronic mail: yutakaohno@imr.tohoku.ac.jp

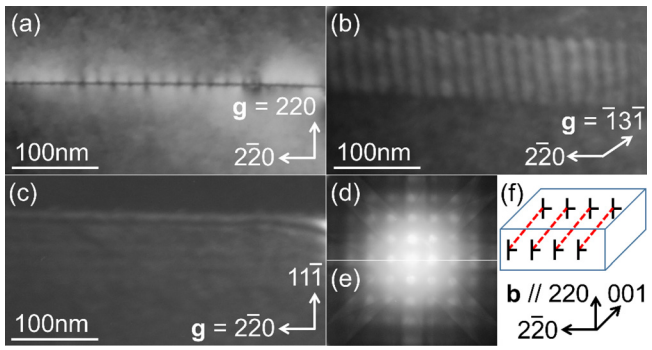

FIG. 1. Dark-field TEM images of a SATB taken with **g** = (a) 220, (b) $\bar{1}3\bar{1}$, and (c) $2\bar{2}0$. The incident directions are (a) [001] and ((b) and (c)) [112]. The [001] transmission electron diffraction patterns of the upper (d) and lower (e) grains in (a). (f) Schematic drawing of the SATB.

with the Integrated Visualization and Analysis Software (IVAS) protocol.[28]

Figure 1 shows TEM data of a grain boundary for APT, whose tilt angle was estimated to be about 1° by EBSD (not shown). Most segments of the boundary laid on (110) (Fig. 1(a)). The boundary was composed of an array of parallel dislocations arranged at intervals of 18 nm, extending toward [001] (Fig. 1(b)). The dislocations were not observed by TEM when the reflection **g** was $2\bar{2}0$ (Fig. 1(c)). Assuming the line direction of [001], they were edge-type dislocations with the Burgers vector **b** of a/2[110] in the FS/RH perfect-crystal convention.[29] In both grains, the [001] zone was close to the 000 spot, indicating that the twist angle of the boundary was almost zero (Figs. 1(d) and 1(e)). The tilt angle was estimated by tracing Kikuchi lines in both grains with an accuracy of about 0.1°. One grain rotated by 1.2° around [001] against the other grain (Figs. 1(d) and 1(e)). The ratio of $|\mathbf{b}|$ to the dislocation interval, $(0.543/\sqrt{2})/18$, corresponded to the tangent of the rotation angle, tan(1.2). Thus, the boundary was confirmed to be a SATB on (110) with $\theta_{SATB} = 1.2°$ (Fig. 1(f)).

Figure 2 shows APT data of a needle with the SATB shown in Fig. 1. Oxygen atoms distributed along parallel

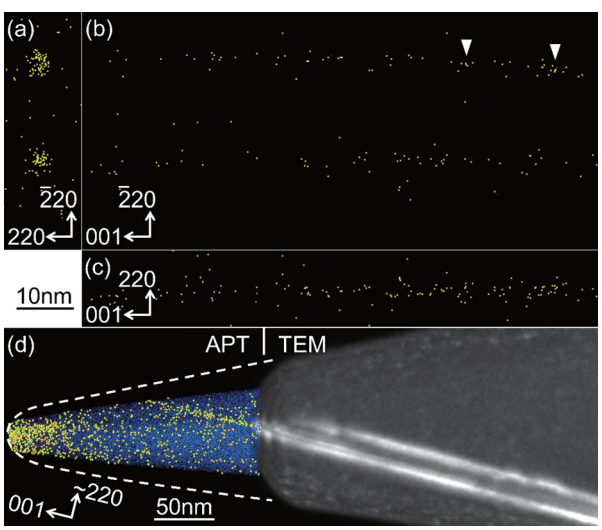

FIG. 2. Projected 3D oxygen maps at the SATB in Fig. 1 in a needle; viewed along (a) [001], (b) [220], and (c) [$\bar{2}$20]. Oxygen atoms in a rectangular prism of $14 \times 40 \times 90\,nm^3$ are plotted. (d) TEM image of the needle after the APT. 3D maps of oxygen (yellow large dots) and Si (blue small dots) atoms are superimposed on the image.

straight lines arranged at intervals of 18 nm, extending toward [001] (Figs. 2(a)–2(c)). A few oxygen clusters less than 1 nm in size (composed of more than three atoms within a volume of $0.5 \times 0.5 \times 0.5\,nm^3$) were formed (e.g., the arrowheads in Fig. 2(b)), while most oxygen atoms were isolated. TEM of the needle after the APT revealed that those lines arranged along the SATB (Fig. 2(d)). Considering the morphological similarity between those lines and edge dislocations composing the boundary, those lines would correspond to the dislocations. Therefore, oxygen atoms would be agglomerated along the dislocation lines in SATBs.

Figures 3(a)–3(d) show projected 3D distribution of oxygen atoms at SATBs with different θ_{SATB}. Two-dimensional (2D) distribution of oxygen density along each dislocation, in a right square prism of $10 \times 10 \times 100\,nm^3$, was calculated (as examples shown in Figs. 3(e)–3(h)), and it could be fitted with a 2D Gaussian function described with the peak density I_{peak} (in at. %) and the standard deviation σ (in nm), $I_{peak} \exp\{-(x^2+y^2)/2\sigma^2\}$. A total of 14 edge dislocations in different SATBs were analysed. Considering the density of Si crystals ($50\,nm^{-3}$), the average number of oxygen atoms at a dislocation per unit dislocation length N_d could be estimated as $\pi\sigma^2 I_{peak}$ (in nm^{-1}). Both σ (Fig. 3(i)) and N_d (Fig. 3(j)) decreased with increasing θ_{SATB}.

Most oxygen atoms agglomerated at dislocations were isolated, indicating that they were likely to be neutral interstitials existing at bond-centered positions in the Si lattice, as observed by infrared spectroscopy. This suggests that the origin of the oxygen gettering would be elastic interactions of SATBs with oxygen atoms, rather than electronic interactions. It is expected that interstitial oxygen atoms can induce compressive stress, since the single-bond covalent radius of Si (0.117 nm) is smaller than that of oxygen (0.070 nm) multiplied by 2 (0.140 nm).[30] Therefore, oxygen atoms were likely to be agglomerated at the tensile side of each

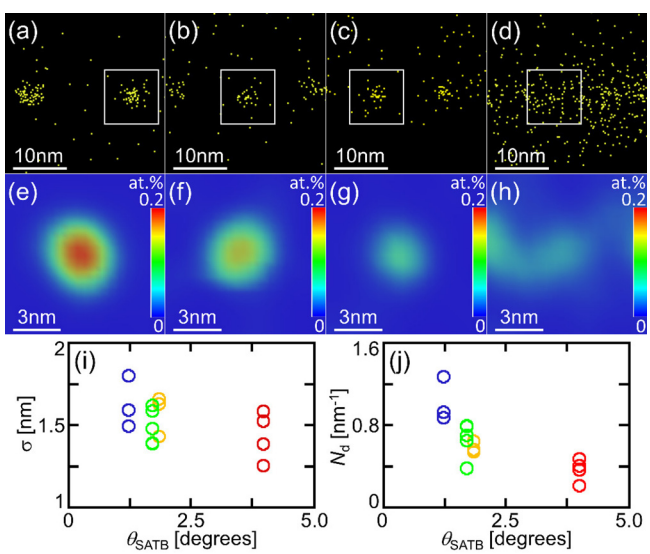

FIG. 3. (a)–(d) Projected 3D oxygen maps viewed along [001] at different SATBs; with the dislocation intervals of (a) 18 nm ($\theta_{SATB} = 1.2°$), (b) 13 nm (1.7°), (c) 12 nm (1.8°), and (d) 5.5 nm (4.0°). Each map plots oxygen atoms in a right square prism with the base parallel to (001) ($30 \times 30 \times 100\,nm^3$). (e)–(h) 2D distribution of the oxygen density in the square areas in (a)–(d). (i) σ vs. θ_{SATB}, and (j) N_d vs. θ_{SATB}.

dislocation core in SATBs, similar to the Cu precipitation at SATBs,[31] though the location of the core was hardly determined by APT. Hereinafter, we discuss the gettering ability in terms of 2D distribution of tensile hydrostatic stress around edge dislocations composing SATBs.

We first discuss the gettering ability of a dislocation composing SATBs. Assuming the dislocation line of $x=y=0$ and the slip plane of $y=0$, the hydrostatic stress around an isolated edge dislocation p is written as[32]

$$p(x,y) = \frac{(1+\nu)\mu b y}{3\pi(1-\nu)(x^2+y^2)}, \quad (1)$$

in which ν is the shear modulus of 80 GPa and μ is the Poisson's ratio of 0.28.[33] Assuming the Burgers vector **b** toward the x direction in the FS/RH perfect-crystal convention, positive $p(x, y)$ for $y>0$ corresponds to be tensile. With this function, the hydrostatic stress at an edge dislocation composing a SATB with θ_{SATB}, P_{SATB} is written as

$$P_{SATB}(x,y,\theta_{SATB}) = \sum_{n=-\infty}^{\infty} p\left(x, y+\frac{b}{\tan(\theta_{SATB})}n\right), \quad (2)$$

in which n is the dislocation number. In SATBs, edge dislocations are arranged so that the compressive strain region of a dislocation faces the tensile strain region of the neighboring dislocation. Therefore, due to the stress compensation effect, the tensile stress around an edge dislocation in SATBs decreases with respect to the tensile stress of the same dislocation in isolation. Contour maps of tensile P_{SATB} for some θ_{SATB} are shown in Figs. 4(a)–4(d). The contour line at a constant stress, depending on θ_{SATB}, can be approximated to be elliptic. The average radius r_{av} decreases with increasing θ_{SATB} (Fig. 4(e)). Comparing Figs. 3(i) and 4(e), about 70% of oxygen atoms agglomerated at SATBs would exist in the atomic sites under the tensile stress larger than 2.0 GPa, so as to reduce the compressive stress due to oxygen atoms. In other words, it is suggested that the critical tensile stress for effective oxygen gettering is about 2.0 GPa.

The area surrounded by the contour line at $P_{SATB}=2.0$ GPa, $S(2.0\,\text{GPa})$, decreases with increasing θ_{SATB} (Fig. 4(f)). The ratio of N_d to $S(2.0\,\text{GPa})$ is almost constant irrespective of θ_{SATB} (about $8\times10^{-2}\,\text{nm}^{-3}$). Therefore, θ_{SATB}-dependent N_d can be explained as the decrease of the gettering sites, under the tensile stress larger than about 2.0 GP, with increasing θ_{SATB}.

We next discuss the gettering ability of SATBs. The average number of oxygen atoms agglomerated at a unit area of a SATB N_{SATB} is estimated as $N_d\tan(\theta_{SATB})/b$ (Fig. 5). Under the above hypothesis that oxygen atoms are agglomerated in the gettering sites under the tensile stress larger than about 2.0 GP, N_d is proportional to $S(2.0\,\text{GPa})$. Therefore, N_{SATB} can be calculated as $8\times10^{-2}S(2.0\,\text{GPa})\tan(\theta_{SATB})/b$ (the solid curve in Fig. 5). It seems that N_{SATB} increases with increasing θ_{SATB}. The gettering ability at $\theta_{SATB}\sim0.5°$ is as small as 30% of that at $\theta_{SATB}\sim2°$, and this may explain the θ_{SATB}-dependence of oxygen-related photoluminescence reported by Tajima *et al.*[3] Also, the θ_{SATB}-dependence of the gettering ability for oxygen is similar to that for iron.[23,34] This suggests the similar gettering mechanism for those impurities. The factor of proportionality, $8\times10^{-2}\,\text{nm}^{-3}$ estimated in the present work, may vary depending on the growth condition in as-grown crystals, as well as on the condition at subsequent annealing.

According to the above hypothesis, it is interesting to note that the gettering ability peaks at $\theta_{SATB}\sim2.5°$ (the solid curve in Fig. 5). When θ_{SATB} is much smaller than the peak angle, $S(2.0\,\text{GPa})$ for a dislocation is mainly affected by the compressive stress due to the neighboring dislocation at the tensile side of the dislocation. Besides, when θ_{SATB} is larger than the peak angle, it is affected by the tensile stress due to the neighboring dislocation at the opposite side, in addition to the above-mentioned compressive stress. The second derivative of $S(2.0\,\text{GPa})$ with respect to θ_{SATB} changes from positive to negative as θ_{SATB} passes the peak angle, and this results in the peaking of the gettering ability. The peak ability may be related to the electrical centers in SATBs with $\theta_{SATB}\sim2°$, reported by Chen and Sekiguchi even in nominally clean crystals for solar cells.[34]

The densities N_{SATB} estimated with the experimental data seem to be close to each other (Fig. 5). As a possible explanation, N_{SATB} may be dynamically limited by diffusion processes of oxygen atoms to SATBs. Under the hypothesis, N_{SATB} would be independent of θ_{SATB}. However, this is contradictory to the result reported by Tajima *et al.*,[3] in which the agglomeration of oxygen atoms were not confirmed at SATBs with $\theta_{SATB}<1°$.

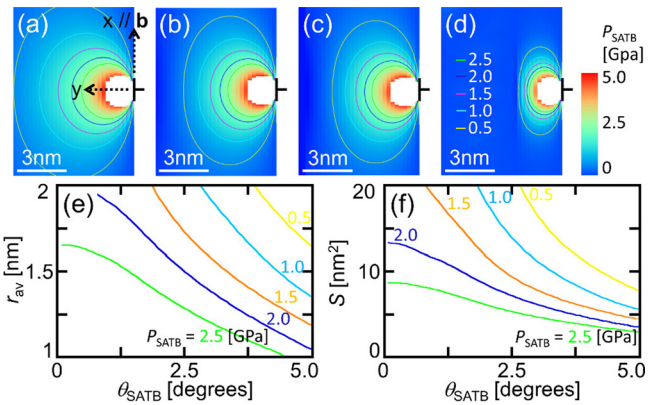

FIG. 4. 2D contour maps of tensile P_{SATB} at a dislocation composing SATBs with $\theta_{SATB}=$ (a) 1.2°, (b) 1.7°, (c) 1.8°, or (d) 4.0°. (e) r_{av} vs. θ_{SATB} and (f) S vs. θ_{SATB} for contour lines at different P_{SATB}.

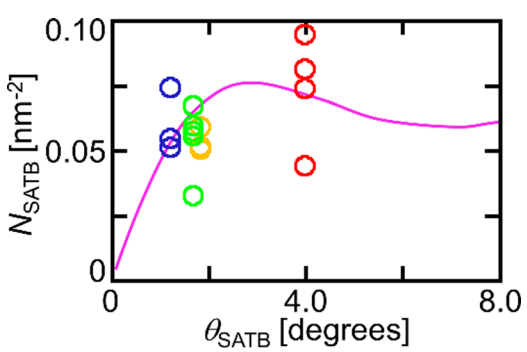

FIG. 5. N_{SATB} vs. θ_{SATB}. The solid curve shows a hypothetic N_{SATB} calculated under the assumption that oxygen atoms are agglomerated in the gettering sites under the tensile stress larger than about 2.0 GP, induced by edge dislocations composing SATBs.

In conclusion, 3D distribution of oxygen atoms at SATBs with different θ_{SATB}, agglomerated during the CZ growth of Si ingots, was examined by APT and TEM. Oxygen atoms would be agglomerated in the atomic sites under the tensile hydrostatic stress larger than about 2.0 GPa induced by edge dislocations composing SATBs. It was under the hypothesis that the density of the gettering sites depending on θ_{SATB} determines the gettering ability of SATBs.

This work was supported by the Integrated Materials Research Center for a Low-Carbon Society in IMR (2012-2014). APT and CZ growth of Si crystals were performed at the Oarai Center and at IMR, respectively, under the Inter-University Cooperative Research Program in IMR.

[1]K. Bothe, K. Ramspeck, D. Hinken, C. Schinke, J. Schmidt, S. Herlufsen, R. Brendel, J. Bauer, J.-M. Wagner, N. Zakharov, and O. Breitenstein, J. Appl. Phys. **106**, 104510 (2009).
[2]M. Di Sabatino, S. Binetti, J. Libal, M. Acciarri, H. Nordmark, and E. J. Ovrelid, Sol. Energy Mater. Sol. Cells **95**, 529 (2011).
[3]M. Tajima, Y. Iwata, F. Okayama, H. Toyota, H. Onodera, and T. Sekiguchi, J. Appl. Phys. **111**, 113523 (2012).
[4]U. Hess, P. Y. Pichon, S. Seren, A. Schonecker, and G. Hahn, Sol. Energy Mater. Sol. Cells **117**, 471 (2013).
[5]J. Haunschild, I. E. Reis, J. Geilker, and S. Rein, Phys. Status Solidi RRL **5**, 199 (2011).
[6]L. Chen, X. Yu, P. Chen, P. Wang, X. Gu, J. Lu, and D. Yang, Sol. Energy Mater. Sol. Cells **95**, 3148 (2011).
[7]J. D. Murphy, R. E. McGuire, K. Bothe, V. V. Voronkov, and R. J. Falster, Sol. Energy Mater. Sol. Cells **120**, 402 (2014).
[8]S. A. McHugo, H. Hieslmair, and E. R. Weber, Appl. Phys. A **64**, 127 (1997).
[9]H. Hieslmair, A. A. Istratov, S. A. McHugo, C. Flink, T. Heiser, and E. R. Weber, Appl. Phys. Lett. **72**, 1460 (1998).
[10]T. Tachibana, T. Sameshima, T. Kojima, K. Arafune, K. Kakimoto, Y. Miyamura, H. Harada, T. Sekiguchi, Y. Ohshita, and A. Ogura, Jpn. J. Appl. Phys., Part 1 **51**, 02BP08 (2012).
[11]R. Falster and V. Voronkov, Mater. Sci. Forum **573–574**, 45–60 (2008).
[12]J. M. Burgers, Proc. K. Ned. Akad. Wet. **42**, 293 (1939).
[13]W. L. Bragg, Proc. Phys. Soc. **52**, 105 (1940).
[14]T. Tachibana, J. Masuda, K. Imai, A. Ogura, Y. Ohshita, K. Arafune, and M. Tajima, Jpn. J. Appl. Phys., Part 1 **48**, 121202 (2009).
[15]K. Kutsukake, M. Deura, Y. Ohno, and I. Yonenaga, "Characterization of silicon ingots: mono-like vs. high-performance multicyrstalline," Jpn. J. Appl. Phys. (in press).
[16]K. Kutsukake, N. Usami, T. Ohtaniuchi, K. Fujiwara, and K. Nakajima, J. Appl. Phys. **105**, 044909 (2009).
[17]M. G. Tsoutsouva, V. A. Oliveira, D. Camel, T. N. TranThi, J. Baruchel, B. Marie, and T. A. Lafford, J. Cryst. Growth **401**, 397 (2014).
[18]K. Kutsukake, T. Abe, N. Usami, K. Fujiwara, I. Yonenaga, K. Morishita, and K. Nakajima, J. Appl. Phys. **110**, 083530 (2011).
[19]M. M. Kivambe, T. Ervik, B. Ryningen, and G. Stokkan, J. Appl. Phys. **112**, 103528 (2012).
[20]G. Kato, M. Tajima, F. Okayama, S. Tokumaru, R. Satod, H. Toyota, and A. Ogura, Acta Phys. Pol. A **125**, 1010 (2014).
[21]T. Walther, M. Hopkinson, N. Daneu, A. Recnik, Y. Ohno, K. Inoue, and I. Yonenaga, J. Mater. Sci. **49**, 3898 (2014).
[22]H. Akutsu, H. Itokawa, K. Nakamura, T. Iinuma, K. Suguro, H. Uchida, and M. Tada, MRS Proceedings **1070**, E02-09 (2008).
[23]T. Sameshima, N. Miyazaki, Y. Tsuchiya, H. Hashiguchi, T. Tachibana, T. Kojima, Y. Ohshita, K. Arafune, and A. Ogura, Appl. Phys. Express **5**, 042301 (2012).
[24]D. P. Fenning, A. S. Zuschlag, M. I. Bertoni, B. Lai, G. Hahn, and T. Buonassisi, J. Appl. Phys. **113**, 214504 (2013).
[25]M. Seibt, D. Abdelbarey, V. Kveder, C. Rudolf, P. Saring, L. Stolze, and O. Vos, Mater. Sci. Eng., B **159–160**, 264 (2009).
[26]T. Buonassisi, A. A. Istratov, S. Peters, C. Ballif, J. Isenberg, S. Riepe, W. Warta, R. Schindler, G. Willeke, Z. Cai, B. Lai, and E. R. Weber, Appl. Phys. Lett. **87**, 121918 (2005).
[27]Y. Ohno, K. Inoue, Y. Tokumoto, K. Kutsukake, I. Yonenaga, N. Ebisawa, H. Takamizawa, Y. Shimizu, K. Inoue, Y. Nagai, H. Yoshida, and S. Takeda, Appl. Phys. Lett. **103**, 102102 (2013).
[28]B. Gault, D. Haley, F. de Geuser, M. P. Moody, E. A. Marquis, D. J. Larson, and B. P. Geiser, Ultramicroscopy **111**, 448 (2011).
[29]D. B. Williams and C. B. Carter, in *Transmission Electron Microscopy* (Plenum Press, New York, 1996), Sec. 25.
[30]R. T. Sanderson, J. Am. Chem. Soc. **105**, 2259 (1983).
[31]Y. Ohno, K. Inoue, K. Kutsukake, M. Deura, T. Ohsawa, I. Yonenaga, H. Yoshida, S. Takeda, R. Taniguchi, H. Otubo, S. R. Nishitani, N. Ebisawa, Y. Shimizu, H. Takamizawa, K. Inoue, and Y. Nagai, Phys. Rev. B **91**, 235315 (2015).
[32]J. P. Hirth and J. Lothe, in *Theory of Dislocations* (John Wiley & Sons, New York, 1982), Secs. 3–4.
[33]J. J. Wortman and R. A. Evans, J. Appl. Phys. **36**, 153 (1965).
[34]J. Chen and T. Sekiguchi, Jpn. J. Appl. Phys., Part 1 **46**, 6489 (2007).